CMS PAS SMP-16-008

CMS Physics Analysis Summary

2017/02/21

Determination of the strong coupling constant from the measurement of inclusive multijet event cross sections in pp collisions at $\sqrt{s} = 8$ TeV

The CMS Collaboration

Abstract

A measurement of inclusive multijet event cross sections is presented from proton-proton collisions recorded at $\sqrt{s} = 8$ TeV with the CMS detector and corresponding to an integrated luminosity of 19.7 fb^{-1}. Jets are reconstructed with the anti-k_t clustering algorithm for a jet size parameter $R = 0.7$ in a phase space region ranging up to jet transverse momenta p_T of 2.0 TeV and an absolute rapidity of $|y| = 2.5$. The inclusive 2-jet and 3-jet event cross sections are measured as a function of the average p_T of the two leading jets. The data are well described by predictions at next-to-leading order in perturbative quantum chromodynamics and additionally are compared to several Monte Carlo event generators. The strong coupling constant at the scale of the Z boson mass is inferred from a fit of the ratio of the 3-jet over 2-jet event cross section giving $\alpha_s(M_Z) = 0.1150 \pm 0.0010\,(\text{exp}) \pm 0.0013\,(\text{PDF}) \pm 0.0015\,(\text{NP})^{+0.0050}_{-0.0000}\,(\text{scale})$.

1 Introduction

Inelastic collisions of protons are viewed as interactions between their constituent partons, the (anti-)quarks and gluons. Within the context of perturbative quantum chromodynamics (pQCD), the cross section of a high-p_T scattering process can be expressed as a sum of terms with increasing powers of the strong coupling constant, α_S, convoluted with the parton momentum distribution functions (PDFs) of the proton. The lowest-order α_S^2 term represents the production of two-parton final states. Terms of higher-order $\alpha_S^3, \ldots$ in the expansion signify the existence of multi-parton final states. The theoretical description of the transition from strongly interacting, colored partons to color-neutral hadrons, which are observable in detectors, relies for this nonperturbative phase on models implemented in Monte Carlo (MC) event generators. To relate the collimated sprays of colorless hadrons to the initiating partons, jet algorithms are applied. These algorithms bundle together particles that are close in phase space and primarily move into the same direction. Hence, the constructed jets preserve energy and momentum of the initial partons so that the structure of the final jet system mirrors, to a large extent, the topology of the initial partonic system.

The inclusive jet cross section, $pp \to jet + X$, as a function of jet p_T and rapidity y is a fundamental observable providing essential information about the PDFs and the strong coupling constant. Corresponding measurements conducted by the experiments at the CERN LHC are reported in Refs. [1–11]. The investigation of inclusive multijet event cross sections $\sigma_{i\to jet}$, $pp \to i\,jets + X$, as suggested here, permits more elaborate tests of QCD to be performed by subdividing the observed jet event sample into classes according to the presumed minimal power in α_S necessary to describe theoretically such a topology. Moreover, the ratios of such cross sections, $R_{nm} = \frac{\sigma_{m\to jet}}{\sigma_{n\to jet}}$, with m > n, are proportional to α_S^{m-n} while at the same time numerous theoretical and experimental uncertainties cancel. Thus, they provide an ideal tool to determine the strong coupling constant $\alpha_s(M_Z)$. A previous analysis of the ratio R_{32} as a function of the average transverse momentum, $\langle p_{T12} \rangle$, of the two leading p_T jets in the event was performed at $\sqrt{s} = 7$ TeV by the CMS Collaboration and lead to an extraction of $\alpha_s(M_Z) = 0.1148 \pm 0.0055$, where the dominant uncertainty stems from the estimation of higher-order corrections to the next-to-leading order (NLO) prediction [12].

In this analysis, a measurement of inclusive 2- and 3-jet event cross sections is presented using an event sample collected by the CMS experiment during 2012 at the LHC and corresponding to an integrated luminosity of 19.7 fb^{-1} of pp collisions at a centre-of-mass energy of 8 TeV. Jets are reconstructed using the infrared- and collinear-safe anti-k_t clustering algorithm [13] with a jet size parameter R of 0.7. All jets are required to satisfy $p_T > 150$ GeV and $|y| < 5.0$. The jet event sample is further reduced by requiring the two leading p_T jets to lie in the central detector region of $|y| < 2.5$.

The event scale is chosen as before to be the average transverse momentum of the two leading jets, but will be referred to as $H_{T12}/2$ in this analysis. Fits of the strong coupling constant are performed for the 2-jet and 3-jet event cross sections separately and for their ratio R_{32}.

2 Event selection and reconstruction

The measurement uses data samples which were collected with six single-jet high-level triggers (HLT) [14]. They are seeded by Level 1 (L1) triggers based on calorimetric information and require at least one jet in the event with corrected jet $p_T > 80, 140, 200, 260,$ and 320 GeV. All except the highest-threshold trigger were prescaled during the 2012 run. The efficiency of each trigger is estimated using lower-p_T-threshold triggers and it is found to be more than 99% in

the $H_{T12}/2$ ranges, shown in Table 1 with the corresponding effective integrated luminosities.

Table 1: Trigger regions defined as ranges of the $H_{T12}/2$ for every single-jet trigger used in the inclusive multijet cross section measurement along with the effective integrated luminosities.

HLT path	$H_{T12}/2$ range (GeV)	Integrated Luminosity (pb^{-1})
PFJet80	120 – 188	2.12
PFJet140	188 – 263	5.57×10
PFJet200	263 – 345	2.61×10^2
PFJet260	345 – 406	1.06×10^3
PFJet320	406 – 5000	1.97×10^4

In the CMS experiment, all particles are reconstructed and identified using a particle-flow (PF) algorithm, which combines the information from the individual subdetectors [15,16]. The four-vectors of particle candidates, reconstructed by the above technique, are used as input to the anti-k_t jet-clustering algorithm. The clustering is performed within the FASTJET package [17] using four-momentum summation.

The reconstructed jets require additional energy corrections to account for residual nonuniformities and nonlinearities in the detector response. These jet energy corrections [18] are derived using simulated events, generated by PYTHIA 6.4 [19] with tune Z2* [20] and processed through the CMS detector simulation based on GEANT4 [21], and in situ measurements with dijet, photon+jet, and Z+jet events. The jet energy corrections, which depend on the η (pseudorapidity) and p_T of the jet, are applied to the jet four-momentum vector as a multiplicative factor [18]. For a jet with a p_T of 100 GeV, the typical correction is about 10%, and decreases with increasing p_T. An additional offset correction is applied to take into account the extra energy clustered into jets from additional proton-proton interactions within the same or neighbouring bunch crossings (in-time and out-of-time pileup) [18]. Pileup effects are important only for jets with low p_T and become negligible for jets with $p_T > 200$ GeV. The current measurement is therefore largely insensitive to pileup effects.

Each selected event is required to have at least one offline-reconstructed vertex [22] along the beam line that is within 24 cm of the nominal interaction point. To suppress nonphysical jets, i.e. jets resulting from noise in the electromagnetic calorimeter (ECAL) and/or the brass/scintillator hadron calorimeter (HCAL), tight identification criteria [23] are applied : each jet should contain at least two particles, one of which is a charged hadron, and the jet energy fraction carried by neutral hadrons and photons should be less than 90%. These criteria have an efficiency greater than 99% for physical jets. Jets not satisfying the tight identification requirements are discarded.

A sample of multijet events is selected which has two or more jets with transverse momentum greater than 150 GeV and $|y| < 5.0$ in the event. Events, in which the two leading p_T jets have $|y| < 2.5$ are selected. Further jets are counted only, if they lie within the same central rapidity range of $|y| < 2.5$.

In QCD, pure jet events are balanced in p_T and thus exhibit a low level of missing transverse energy, which predominantly is caused by jet calibration and resolution effects of the detector. Therefore, the ratio of missing transverse energy to the total transverse energy $\frac{E_T^{miss}}{\sum E_T}$, both derived from the reconstructed particle-flow objects, is required to be less than 0.3 to select well measured jet events.

3 Measurement of the inclusive 2-jet and 3-jet event cross sections

The inclusive differential multijet cross sections are measured as a function of the average transverse momentum, $H_{T,2}/2 = \frac{1}{2}(p_{T,1} + p_{T,2})$, where $p_{T,1}$ and $p_{T,2}$ denote the transverse momenta of the two leading jets. For inclusive 2-jet events sufficient data are available up to $H_{T,2}/2 = 2$ TeV, while for inclusive 3-jet events (and the ratio R_{32}) the accessible range in $H_{T,2}/2$ is limited to $H_{T,2}/2 < 1.68$ TeV. In the following, results for the inclusive 2-jet and 3-jet event selections will be labelled as $n_j \geq 2$ and $n_j \geq 3$, respectively.

The inclusive differential jet event cross section is defined as :

$$\frac{d\sigma}{d(H_{T,2}/2)} = \frac{1}{\epsilon \mathcal{L}_{int,eff}} \frac{N_{event}}{\Delta(H_{T,2}/2)} \qquad (1)$$

where ϵ is the product of the trigger and jet selection efficiencies, which are greater than 99%, $\mathcal{L}_{int,eff}$ is the effective integrated luminosity, N_{event} is the number of 2- or 3-jet events counted in an $H_{T,2}/2$ bin, and $\Delta(H_{T,2}/2)$ are the bin widths. The measurements are reported in units of (pb/GeV).

To compare the measured cross sections with theoretical predictions at particle level, an unfolding procedure based on the iterative D'Agostini method [24] as implemented in the RooUn-FOLD software package [25] is applied. This correction for detector resolution effects is regularized by an early stopping after four iterations similarly as in a previously published 3-jet measurement [26], which prevents the buildup of large-scale correlations. The response matrix describes the mapping between the particle-level $H_{T,2}/2$ spectrum and the reconstructed $H_{T,2}/2$ spectrum. To construct the response matrix, the particle-level $H_{T,2}/2$ spectrum is taken from a fit to the theoretically predicted $H_{T,2}/2$ spectrum. The reconstructed $H_{T,2}/2$ spectrum is obtained by smearing this particle-level prediction. The resolution in $H_{T,2}/2$ is evaluated from CMS detector simulation based on the MADGRAPH5 + PYTHIA6 MC event generator using a jet-based smearing according to the jet energy resolution (JER). The JER from simulation is corrected (increased) for residual differences between data and simulation following Ref. [18].

Figure 1 shows the response matrices derived using a Toy MC procedure for inclusive 2-jet (left) and 3-jet events (right). The matrices are normalized to the number of generated events in each column and are mostly diagonal with small off-diagonal elements describing migrations between close-by $H_{T,2}/2$ bins.

Through the unfolding procedure the final statistical uncertainties become correlated among bins. The size of these correlations varies typically between 10 and 20%. As a consequence, statistical fluctuations present in data before the unfolding might affect neighbouring bins after the unfolding. The fluctuations observed in the unfolded spectrum are compatible with the statistical uncertainties of the underlying detector-level distributions and the statistical uncertainty after unfolding increases with respect to the original one of the measured data.

The unfolding procedure is affected by uncertainties of the JER. Alternative response matrices, which were built by varying the JER one standard deviation up and down [18], are used to unfold the measured spectra for comparison and introduce a corresponding uncertainty on the cross sections. In addition, to account for a model dependence of the theoretical $H_{T,2}/2$ spectrum, two different functions are assumed when fitting the theoretically predicted $H_{T,2}/2$ spectra. Finally, a supplementary uncertainty is attributed by comparison to an unfolding with a 30% reduced resolution as compared to the one extracted from simulation. This accounts for shortcomings in the detector simulation of the theory spectra leading to small nonclosures

observed in the unfolding. All three uncertainties are added quadratically to give the unfolding uncertainty, which increases from about 1% at low $H_{T,2}/2$ up to 2% at the high $H_{T,2}/2$ end of the cross sections.

The dominant detector-related contribution to the experimental systematic uncertainty of the measured cross sections is caused by the jet energy corrections (JEC) [18]. The JEC uncertainty ranges for inclusive 2-jet events from 3% to 10% and for inclusive 3-jet events from 3% to 8%, respectively.

The uncertainty on the integrated luminosity, which propagates directly to the cross sections, is 2.6% [27] and at low $H_{T,2}/2$ is of a similar size as the one from the JEC. To account for residual effects of small inefficiencies from triggering and jet identification, an uncorrelated uncertainty of 1% is assumed across all $H_{T,2}/2$ bins, similar as in previous CMS jet cross-section measurements [8].

The total experimental systematic uncertainty on the measured cross section is obtained by summing in quadrature the single contributions. The upper panels of Fig. 2 give an overview of all experimental uncertainties affecting the cross section measurement for inclusive 2-jet (top left) and 3-jet events (top right). The error bars indicate the statistical uncertainty after unfolding. The colored lines represent the systematic uncertainties resulting from JEC, the luminosity, residual effects, and the unfolding including JER effects. The total experimental uncertainty, indicated by dashed black lines, is calculated by adding in quadrature all the sources of uncertainty. Beyond about 1.4 (1.2) TeV the statistical uncertainty is dominating for the 2-jet (3-jet) event cross sections, respectively.

The cross section ratio R_{32} as a function of $H_{T,2}/2$ is extracted from the ratio of unfolded differential cross sections for each bin in $H_{T,2}/2$. The systematic experimental uncertainties are propagated from the cross sections to the ratio taking into account correlations. The uncertainties due to luminosity and residual effects cancel completely in this ratio. The statistical uncertainty including bin-by-bin correlations and statistical correlations between the 3-jet and 2-jet event cross sections is derived by directly unfolding the measured ratio R_{32}. Figure 2 "bottom panel" presents an overview of all experimental uncertainties affecting the cross section ratio R_{32}. The JEC and unfolding uncertainties for R_{32} amount to about 1-2% and $\approx 1\%$, respectively. The total uncertainty, calculated by adding in quadrature all individual sources of uncertainty, is dominated by statistical effects beyond about 0.8 TeV in $H_{T,2}/2$.
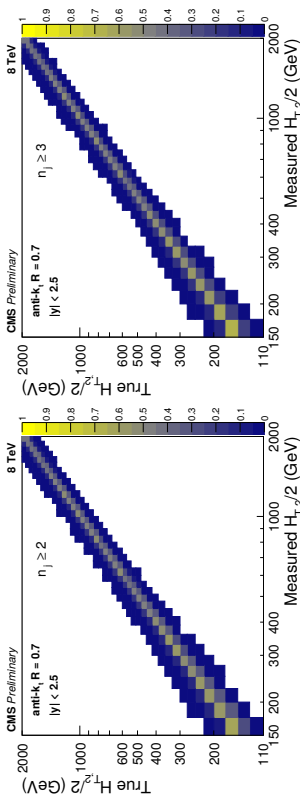
Figure 1: Response matrices derived using a Toy MC procedure for the inclusive 2-jet (left) and 3-jet event samples (right).
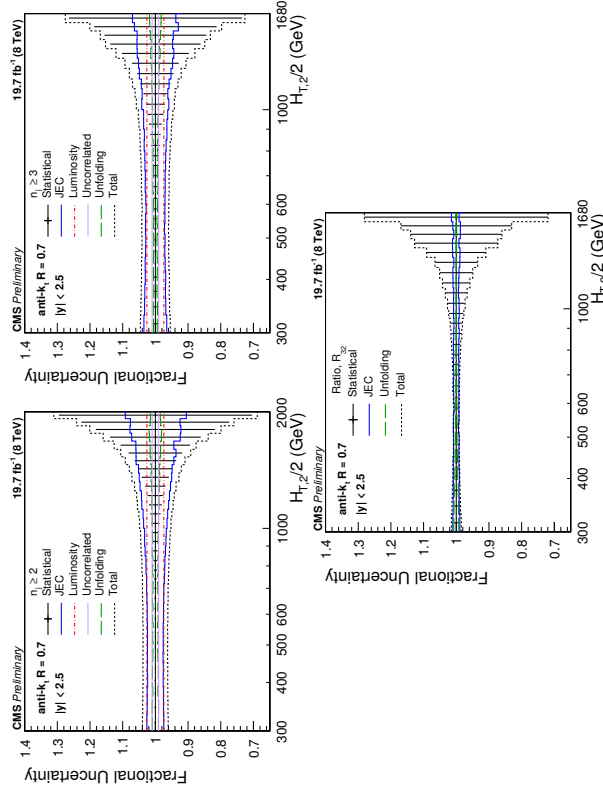
Figure 2: Overview of all experimental uncertainties affecting the inclusive 2-jet (top left) and 3-jet event cross sections (top right) and their ratio R_{32} (bottom). The error bars indicate the statistical uncertainty after unfolding. The colored lines represent the systematic uncertainties resulting from JEC, the luminosity, residual effects, and the unfolding including JER effects. Uncertainties due to luminosity and residual effects are cancelled completely in the ratio. The total experimental uncertainty, indicated by dashed black lines, is calculated by adding in quadrature all the sources of uncertainty.

4   Theory predictions

Predictions at NLO accuracy in pQCD are computed with the NLOJET++ program version 4.1.3 [28, 29]. The results are provided within the framework of FASTNLO version 2.3 [30] for use within fits. The renormalization and factorization scales μ_r and μ_f are chosen equal to $H_{T_2}/2$. PDF sets at NLO available for a series of different assumptions on $\alpha_s(M_Z)$ via the LHAPDF6 package [31] are listed in Table 2. All sets employ a variable-flavour number scheme with at most five or six flavours apart from the ABM11 PDFs, which use a fixed-flavour number scheme with $N_F = 5$.

Out of these eight PDF sets the following three will not be considered further:

• At NLO, predictions based on ABM11 do not describe LHC jet data at small jet rapidity, cf. Refs. [4, 5, 26, 32].

• The HERAPDF2.0 set exclusively fits HERA DIS data with only weak constraints on the gluon PDF.

• The range in values available for $\alpha_s(M_Z)$ is too limited for the NNPDF3.0 set.

PDF uncertainties are evaluated according to the prescriptions given for each PDF set. Uncertainties on $\alpha_s(M_Z)$ are not considered, since this value is later on determined from a fit to the data. The PDF uncertainty as derived with the CT10 PDF set ranges from 2% to 30% for inclusive 2- and 3-jet cross sections and from 2% to 7% for R_{32}.

Table 2: NLO PDF sets available via LHAPDF6 for comparisons to data with various assumptions on the value of $\alpha_s(M_Z)$. Sets existing already in LHC Run 1 (upper rows) and newer sets for Run 2 (lower rows) are listed together with the corresponding number of flavours N_F, the assumed masses M_t and M_Z of the top quark and the Z boson, respectively, the default values of $\alpha_s(M_Z)$, and the range in $\alpha_s(M_Z)$ variation available for fits. A * behind the $\alpha_s(M_Z)$ values signifies that the parameter was fixed, not fitted.

Base set	Refs.	N_F	M_t (GeV)	M_Z (GeV)	$\alpha_s(M_Z)$	$\alpha_s(M_Z)$ range
ABM11	[33]	5	180	91.174	0.1180	0.110–0.130
CT10	[34]	≤5	172	91.188	0.1180*	0.112–0.127
MSTW2008	[35, 36]	≤5	10^{10}	91.1876	0.1202	0.110–0.130
NNPDF2.3	[37]	≤6	175	91.1876	0.1180*	0.114–0.124
CT14	[38]	≤5	172	91.1876	0.1180*	0.113–0.123
HERAPDF2.0	[39]	≤5	173	91.1876	0.1180*	0.110–0.130
MMHT2014	[40]	≤5	10^{10}	91.1876	0.1180*	0.108–0.128
NNPDF3.0	[41]	≤5	173	91.2	0.1180*	0.115–0.121

The uncertainty related to unknown higher orders of the perturbative series is evaluated with the conventional recipe of varying the default scale $H_{T_2}/2$ chosen for μ_r and μ_f independently in the following six combinations: $(\mu_r/H_{T_2}/2, \mu_f/H_{T_2}/2) = (1/2,1/2), (1/2,1), (1,1/2), (1,2), (2,1)$ and $(2,2)$. The maximal upwards and downwards deviations in cross section from the central prediction are taken as scale uncertainty. This uncertainty ranges for inclusive 2-jet events from 5% to 13%, for inclusive 3-jet events from 11% to 17% and for their ratio R_{32} from 6% to 8%.

The computation of the NLO predictions with NLOJET++ is also subject to statistical fluctuations from the numerical integrations. For the inclusive 2-jet event cross sections this uncer-

tainty is smaller than about one per mille, while for the inclusive 3-jet event cross section it amounts to 1–9 per mille.

Higher order effects of electroweak origin affect jet cross sections at large jet p_T. These electroweak (EWK) corrections have been calculated for the inclusive 1-jet and 2-jet case, cf. Ref. [42], but are not yet known for 3-jet production. Therefore, they are considered for the 2-jet events, while for the 3-jet event cross section and for the ratio they have been neglected.

The impact of nonperturbative (NP) effects, i.e. from multiple-parton interactions (MPI) and hadronization, are evaluated by using samples obtained from different MC event generators with a simulation of parton-shower and underlying-event (UE) contributions. The leading order (LO) MC event generators HERWIG++ [43] with the default tune of version 2.3 and PYTHIA6 [19] with tune Z2* are considered, and the dijet NLO prediction from POWHEG [44–46] interfaced to PYTHIA8 with tune CUETS1 [47] for full event generation. The cross section ratios between a nominal event generation and a sample without hadronization and MPI effects are taken as correction separately for inclusive 2-, and 3-jet events, and as their ratio for R_{32}. This ratio is fitted by a power-law function. The differences in the correction factors obtained from the various MC event generators are assigned as an uncertainty. The central correction factors C^{NP} are determined by the centre of the envelope which covers all predictions and half of the spread is taken as the uncertainty.
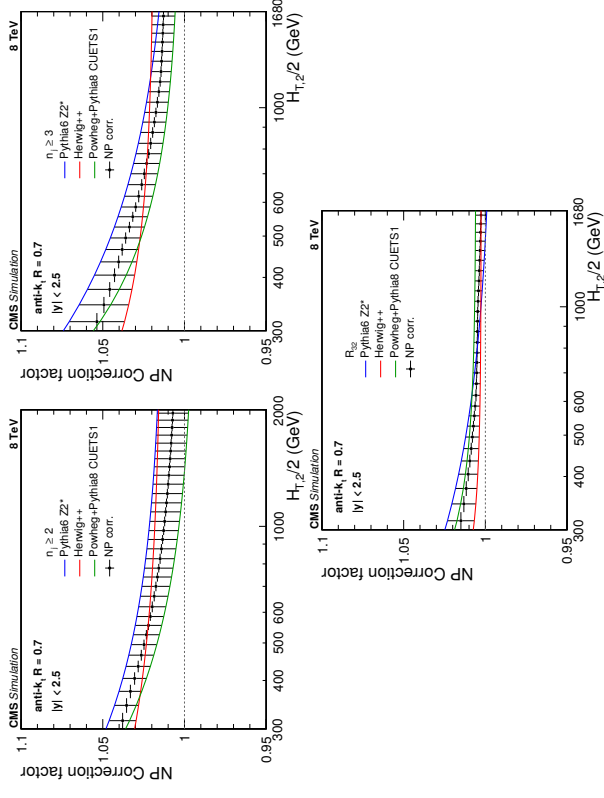
Figure 3: Fits to the nonperturbative corrections obtained for inclusive 2-jet (top left) and 3-jet (top right) event cross sections and their ratio R_{32} (bottom) as a function of $H_{T2}/2$ within $|y| < 2.5$ for the three investigated MC event generators.

The NP corrections are shown in Fig. 3 for the inclusive 2-jet (top left) and 3-jet event cross

sections (top right) as well for R_{32} (bottom). They amount to $\approx$ 4–5% for inclusive 2-jet and 3-jet events and $\approx$ 1% for R_{32} at $H_{T2}/2 \approx 300$ GeV and decrease for increasing $H_{T2}/2$. The uncertainty assigned to the NP corrections is of the order of 1–2%. The non-perturbative effects are reduced in the cross section ratio.
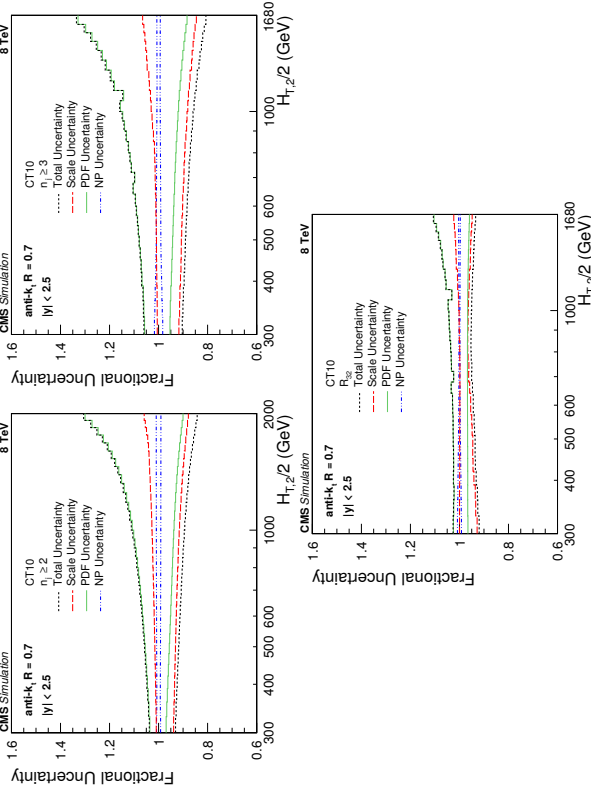
Figure 4: Overview of theoretical uncertainties affecting the cross section prediction for inclusive 2-jet (top left) and 3-jet events (top right) and their ratio R_{32} (bottom), using the CT10 PDF set. The total uncertainty is calculated by adding in quadrature the individual sources of uncertainty. The statistical uncertainties of the NLO computations are too small to be visible and are not shown.

The total theoretical uncertainties are evaluated as the quadratic sum of the scale, PDF, NP, and statistical uncertainties. Figure 4 presents an overview of the theoretical uncertainties affecting the cross section prediction for inclusive 2-jet (top left) and 3-jet events (top right) and their ratio R_{32} (bottom), using the CT10 PDF set.

5   Comparison between measured cross sections and theory

Figure 5 shows the measured inclusive 2-jet and 3-jet event cross sections as a function of $H_{T2}/2$ after unfolding for detector effects. On the left, the measurements are compared to the NLO-JET++ predictions using the CT10 PDF set, corrected for NP effects and in addition for EWK effects in the 2-jet case. On the right, the comparison is made to the predictions from MAD-GRAPH5 + PYTHIA6 with tune Z2* (MG+P6 Z2*), corrected for EWK effects in the 2-jet case. On a logarithmic scale, the data are in agreement with the NLO predictions over the whole
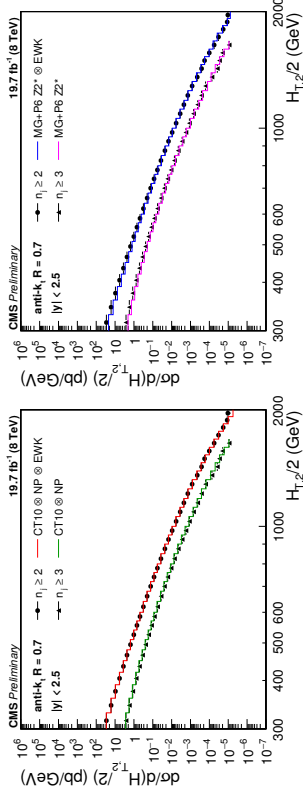
Figure 5: Comparison of the inclusive 2-jet and 3-jet event cross sections as a function of $H_{T,2}/2$ to theoretical predictions. On the (left), the data (points) are shown together with NLOJET++ predictions (line) using the CT10 PDF set, corrected for NP and EWK (2-jet) or only NP effects (3-jet). On the (right), the data (points) are compared to predictions from MADGRAPH5 + PYTHIA6 with tune Z2* (line), corrected for EWK effects in the 2-jet case. The error bars correspond to the total uncertainty, for which the statistical and systematic uncertainties are added in quadrature.

Figure 6: Ratio of data over theory using the CT10 PDF set for inclusive 2-jet (top left) and inclusive 3-jet event cross sections (top right) and their ratio R_{32} (bottom). For comparison predictions employing two other PDF sets are also shown. The error bars correspond to the statistical uncertainty of the data and the shaded rectangles to the total experimental systematic uncertainty. The shaded band around unity represents the total uncertainty of the theory.

range of $H_{T,2}/2$ from 300 GeV up to 2.0 (2-jet) and 1.68 TeV (3-jet) respectively.

For better visibility the ratios of data over the NLOJET++ predictions using the CT10 PDF set are shown in Fig. 6. The data are well described by the predictions within their uncertainty, which is dominated at large $H_{T,2}/2$ by PDF effects in the upwards and by scale variations in the downwards direction. A trend towards an increasing systematic excess of the 2-jet data with respect to theory, starting at about 1 TeV in $H_{T,2}/2$, is remedied by the inclusion of EWK corrections. In the 3-jet case the statistical precision of the data and the reach in $H_{T,2}/2$ is insufficient to observe any effect. The alternative PDF sets MSTW2008 and NNPDF2.3 exhibit a small underestimation of the cross sections at high $H_{T,2}/2$.

As for the NP corrections, the POWHEG framework providing a NLO dijet calculation matched to the parton showers of PYTHIA8 is used for a comparison. Here, POWHEG + PYTHIA8 are employed with the CUETS1 and CUETM1 tunes. The ratios of data over theory from POWHEG + PYTHIA8 with tune CUETS1 are shown in Fig. 7. For comparison, the LO prediction from PYTHIA8 with tune Z2*, the tree-level multi-leg improved prediction by MADGRAPH5 + PYTHIA6 with tune Z2*, and the matched NLO prediction from POWHEG + PYTHIA8 with tune CUETM1 are shown as well. Significant discrepancies, which are cancelled to a large extent in the ratio R_{32}, are visible in the comparison with the LO prediction from MADGRAPH5 + PYTHIA6 with tune Z2*, in particular for small $H_{T,2}/2$. In contrast, the employed dijet MC PYTHIA8 and POWHEG + PYTHIA8 better describe the 2-jet event cross section, but fail for the 3-jet case.

The cross section ratio R_{32} as a function of $H_{T,2}/2$ is extracted from the data by dividing the differential cross sections for each bin in $H_{T,2}/2$. Figure 8 presents this ratio as obtained from unfolded data in comparison to that from NLO pQCD. The error bars correspond to the total experimental uncertainty.

For a better comparison of the behaviour of the 2- and 3-jet event cross sections and their ratio Figs. 9–11 present the respective ratios with respect to theory for varying assumptions on PDFs and $\alpha_s(M_Z)$. A small slope increasing with $H_{T,2}/2$ is visible for most PDFs in both cross
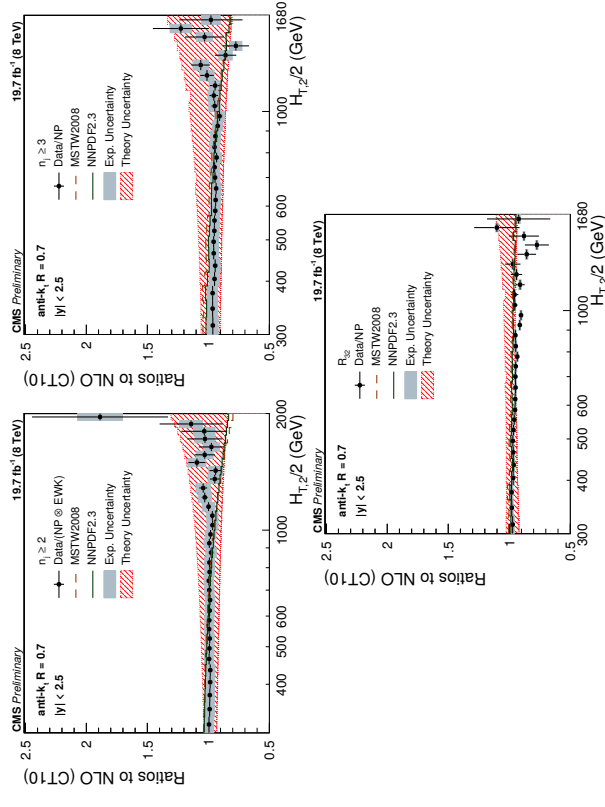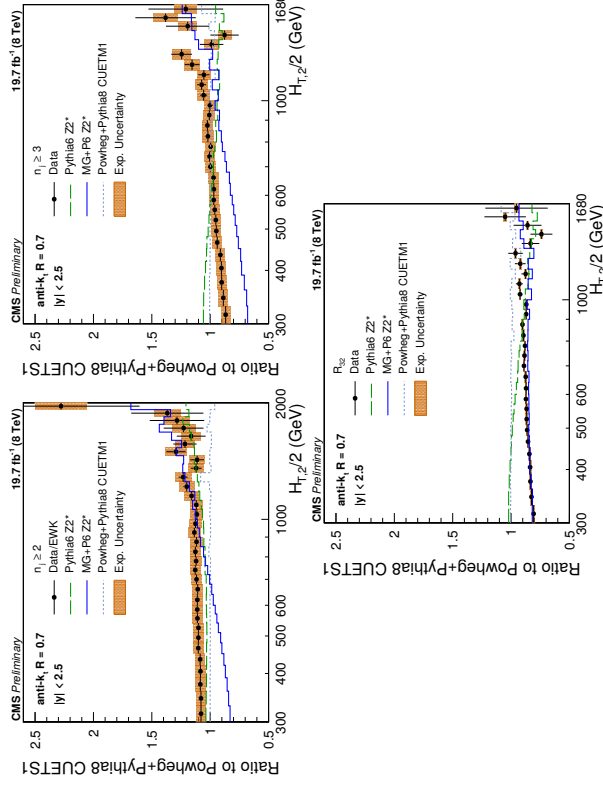
Figure 7: Ratio of data over the prediction from POWHEG + PYTHIA8 with tune CUETS1. For comparison the alternative tune CUETM1 of POWHEG + PYTHIA8, the tree-level multi-leg improved prediction by MADGRAPH5 + PYTHIA6 with tune Z2*, and the LO MC predictions from PYTHIA6 tune Z2* are shown as well. The error bars correspond to the statistical uncertainty of the data and the shaded rectangles to the total experimental systematic uncertainty. EWK corrections have been accounted for in this comparison in the 2-jet case.
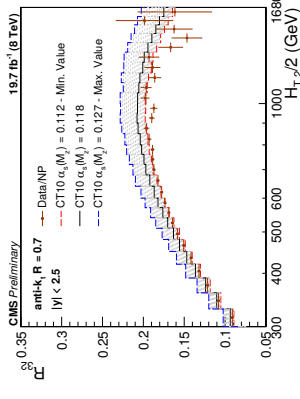
Figure 8: Cross section ratio R_{32} as a function of $H_{T2}/2$ calculated from data (solid circles) in comparison to that from NLO pQCD (lines). The error bars correspond to the total experimental uncertainty derived as quadratic sum from all uncertainty sources. The NLO predictions using the CT10 NLO PDF set corrected with NP corrections are shown for a series of values assumed for $\alpha_s(M_Z)$ (dashed lines) together with the central prediction (solid line) where $\alpha_s(M_Z) = 0.118$. The assumption on $\alpha_s(M_Z)$ is varied in steps of 0.001 in the range of 0.112–0.127. For brevity, the relative factor of NP between data and theory has been indicated as "Data/NP" in the legend.

sections. This effect is largely cancelled in the cross section ratio. R_{32} exhibits a flat behaviour with respect to the predictions for all five PDF sets in the whole range of $H_{T2}/2$ up to 1.68 TeV.

Moreover, the different sensitivity to $\alpha_s(M_Z)$ caused by the leading power in α_S in the expansion of the 2-jet inclusive ($\propto \alpha_S^2$) and the 3-jet inclusive cross section ($\propto \alpha_S^3$), and their ratio ($\propto \alpha_S^1$) is clearly visible from the spread between the calculations for the smallest and largest value of $\alpha_s(M_Z)$ within the same PDF set when passing through Figs. 9–11. This also demonstrates the potential of ratios R_{nm} with $m - n > 1$.

6   Fits of the strong coupling constant

As discussed in the previous section, the measured inclusive 2-jet and 3-jet event cross sections and their ratio R_{32} can be used for a determination of the strong coupling constant $\alpha_s(M_Z)$. The value of $\alpha_s(M_Z)$ is determined by minimizing the χ^2 between the experimental measurement and the theoretical predictions. The fit procedure here follows closely the one previously used in Refs. [12] and [48]. The χ^2 is defined as:

$$\chi^2 = M^T C^{-1} M,$$ (2)

where M is the vector of the differences between the data (D^i) and the theoretical values (T^i) in each bin i,

$$M^i = D^i - T^i$$ (3)

and C is the covariance matrix including all experimental uncertainties as described in Section 3 and some theoretical uncertainties. More precisely, $C = C_{exp} + C_{theo}$ is defined as the sum of

Figure 10: Ratio of measured 3-jet inclusive event cross section (data points) over NLO theory times NP corrections for various PDF sets at their respective default value for $\alpha_s(M_Z)$ (black solid line at unity). The error bars correspond to the total experimental uncertainty. The NLO predictions have been derived with the CT10 (top left), the CT14 (top right), the MSTW2008 (middle left), the MMHT2014 (middle right) and the NNPDF2.3 PDF sets (bottom) for the series of assumptions on $\alpha_s(M_Z)$ available for the respective PDF set as specified in Table 2. For brevity, the relative factor of NP between data and theory has been indicated as "Data/NP" in the legend.

Figure 9: Ratio of measured 2-jet inclusive event cross section (data points) over NLO theory times NP corrections for various PDF sets at their respective default value for $\alpha_s(M_Z)$ (black solid line at unity). The error bars correspond to the total experimental uncertainty. The NLO predictions have been derived with the CT10 (top left), the CT14 (top right), the MSTW2008 (middle left), the MMHT2014 (middle right) and the NNPDF2.3 PDF sets (bottom) for the series of assumptions on $\alpha_s(M_Z)$ available for the respective PDF set as specified in Table 2. For brevity, the relative factor of NP between data and theory has been indicated as "Data/NP" in the legend.

covariances of experimental and theoretical sources of uncertainty as follows

$$C_{exp} = Cov^{ExpStat} + \sum Cov^{JEC} + Cov^{Unfolding} + Cov^{Lumi} + Cov^{Uncor} , \qquad (4)$$

$$C_{theo} = Cov^{TheoStat} + Cov^{NP} + Cov^{PDF} , \qquad (5)$$

where the labelled covariance matrices account for the following effects:

- $Cov^{ExpStat}$: the statistical uncertainty of the data including correlations introduced by the unfolding,

- Cov^{JEC}: the JEC systematic uncertainty,

- $Cov^{Unfolding}$: the unfolding systematic uncertainty including the JER,

- Cov^{Lumi}: the luminosity uncertainty,

- Cov^{Uncor}: a residual uncorrelated systematic uncertainty summarizing individual causes such as trigger and identification inefficiencies, time dependence of the jet p_T resolution, and uncertainty on the trigger prescale factors,

- $Cov^{TheoStat}$: the statistical uncertainty caused by numerical integrations in the cross section computations,

- Cov^{NP}: the systematic uncertainty of the NP corrections, and

- Cov^{PDF}: the PDF uncertainty.

In fits of the ratio R_{32}, the luminosity and residual uncorrelated uncertainties cancel completely. Partial cancellations between the other sources of uncertainty are taken into account in the fit. The JEC, unfolding, and luminosity uncertainties are treated as multiplicative to avoid the statistical bias that arises when estimating uncertainties from data.

The derivation of PDF uncertainties depends on each PDF set. The CT10 PDF set consists of $N_{ev} = 26$ eigenvectors with two PDF members per eigenvector k, which lead to the predictions $S_k^{\pm}$ that follow from PDF variations with respect to the plus and minus directions of eigenvector k. Symmetric uncertainties as required by the use of covariance matrices are then computed by [49]:

$$(\Delta X)^2 = \frac{1}{4} \sum_{k=1}^{N_{ev}} [X(S_k^+) - X(S_k^-)]^2 , \qquad (6)$$

where ΔX is the uncertainty of the cross section and $X(S_k^{\pm})$ is the predicted cross section for each eigenvector orientation, $+$ or $-$.

Scale uncertainties of the pQCD predictions are taken into account employing the offset method, i.e. by performing separate fits with varying scale factors as described in the previous section. The largest upwards and downwards deviations from the default factors are defined as the uncertainty. At NLO such scale variations predominantly lead to smaller cross sections and also a smaller ratio R_{32} as visible in Fig. 4. As a consequence the scale uncertainty in fits is equally asymmetric, where smaller cross sections or ratios are compensated by an increase in the fitted value for $\alpha_s(M_Z)$.

First, fits to the cross sections are performed, where the range in $H_{T,2}/2$ is restricted to be between 300 GeV and 1 TeV to avoid the region close to the minimal p_T threshold of 150 GeV for each jet at low p_T and the onset of electroweak effects at high p_T, which are available for
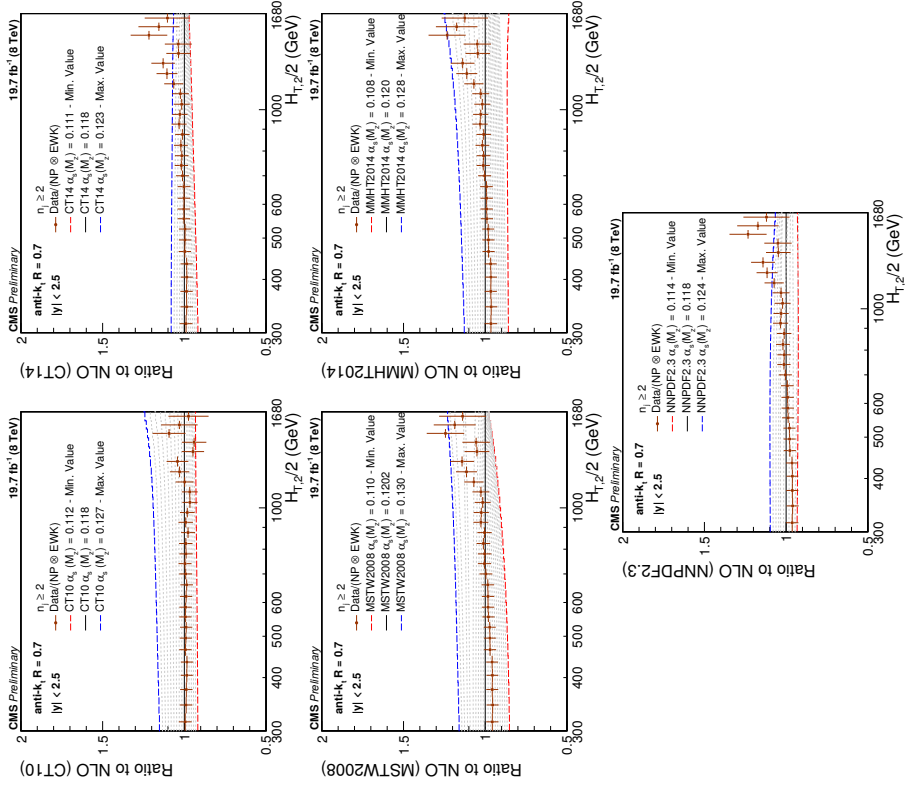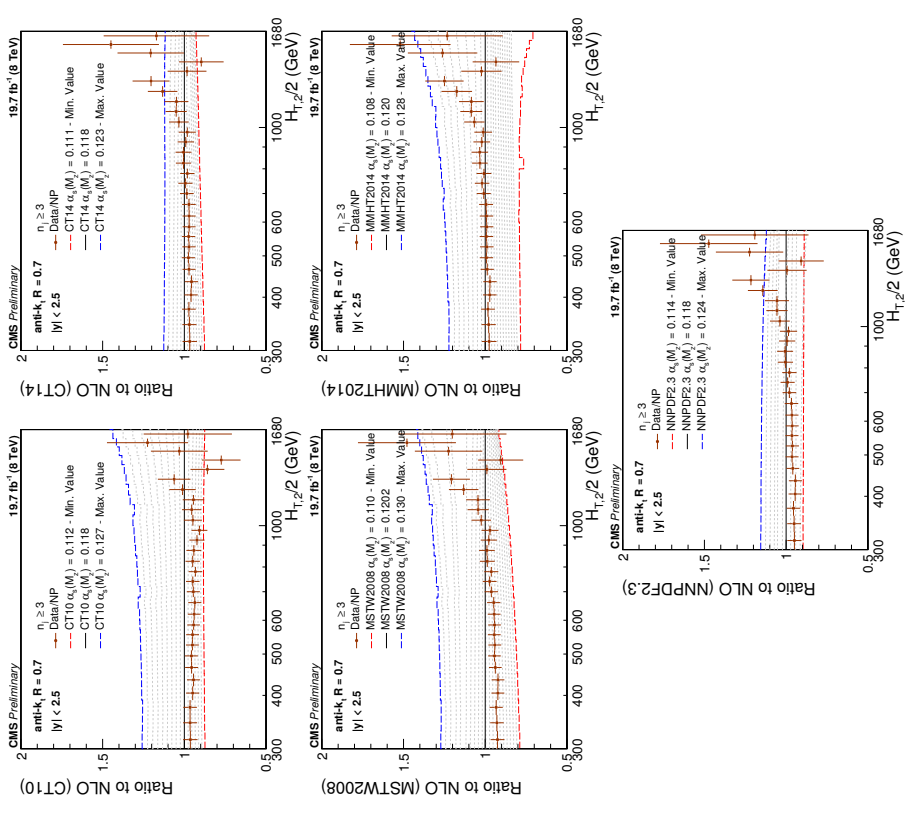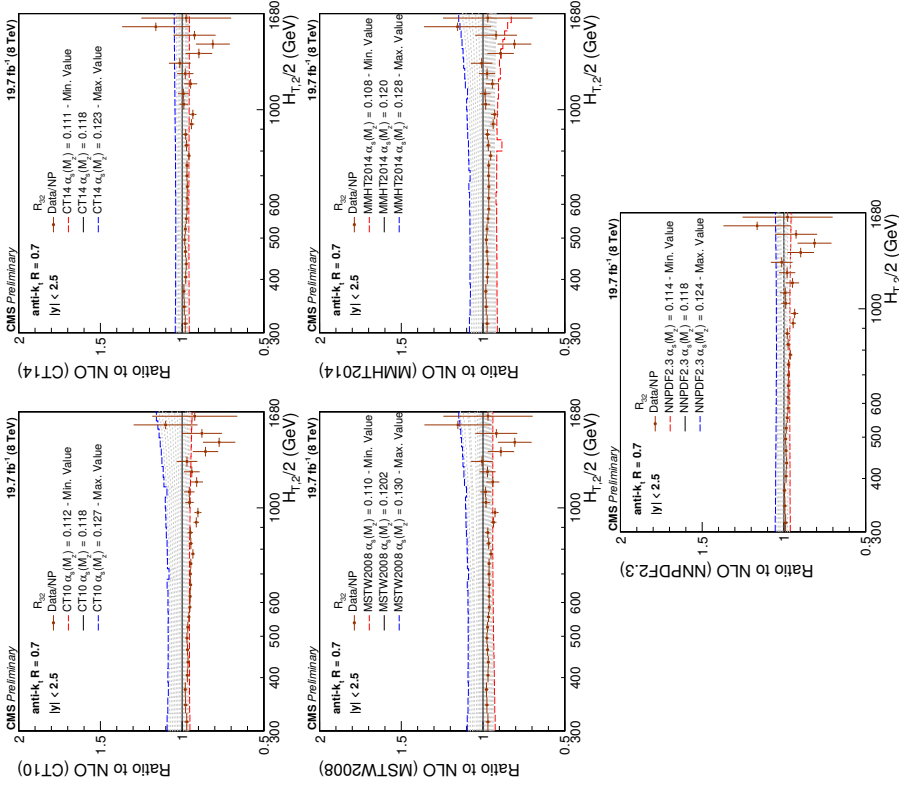
Figure 11: Ratio of measured R_{32} ratio (data points) over NLO theory times NP corrections for various PDF sets at their respective default value for $\alpha_s(M_Z)$ (black solid line at unity). The error bars correspond to the total experimental uncertainty. The NLO predictions have been derived with the CT10 (top left), the CT14 (top right), the MSTW2008 (middle left), the MMHT2014 (middle right) and the NNPDF2.3 PDF sets (bottom) for the series of assumptions on $\alpha_s(M_Z)$ available for the respective PDF set as specified in Table 2. For brevity, the relative factor of NP between data and theory has been indicated as "Data/NP" in the legend.

the dijet case only. The results are reported in Table 3 for the 2-jet and 3-jet event cross sections. For comparison, a simultaneous fit to both cross sections ignoring any correlations, and a fit to their ratio fully accounting for correlations are given in Table 4. Also, EWK effects are assumed to cancel in the ratio as do the luminosity and the uncorrelated uncertainty.

All cross section fits give compatible values for $\alpha_s(M_Z)$ in the range of 0.115–0.118; for the ratio R_{32} somewhat smaller values are obtained. A common issue, except for the ratio fits, is the rather small χ^2/n_{dof}. A possible explanation is an overestimation of the residual uncorrelated uncertainty of 1% that is cancelled for R_{32}. If the fits are repeated with an assumed uncertainty of 0.25% instead, the χ^2/n_{dof} values lie around unity while the $\alpha_s(M_Z)$ values are still compatible with the previous results but with slightly reduced uncertainties.

Table 3: Determination of $\alpha_s(M_Z)$ from the inclusive 2-jet and 3-jet event cross sections using five PDF sets at NLO. Only total uncertainties without scale variations are quoted. The results are obtained from a simultaneous fit to all 19 $H_{T2}/2$ bins in the restricted range of $0.3 < H_{T2}/2 < 1.0$ TeV.

PDF set	2-jets			3-jets		
	$\alpha_s(M_Z)$	$\pm\Delta\alpha_s(M_Z)$	χ^2/n_{dof}	$\alpha_s(M_Z)$	$\pm\Delta\alpha_s(M_Z)$	χ^2/n_{dof}
CT10	0.1174	0.0032	3.0/18	0.1169	0.0027	5.4/18
CT14	0.1160	0.0035	3.5/18	0.1159	0.0031	6.1/18
MSTW2008	0.1159	0.0025	5.3/18	0.1161	0.0021	6.7/18
MMHT2014	0.1165	0.0034	5.9/18	0.1166	0.0025	7.1/18
NNPDF2.3	0.1183	0.0025	9.7/18	0.1179	0.0021	9.1/18

Table 4: Determination of $\alpha_s(M_Z)$ from the inclusive 2-jet and 3-jet event cross sections simultaneously and from their ratio R_{32} using five PDF sets at NLO. Only total uncertainties without scale variations are quoted. The results are obtained from a simultaneous fit to all 38 (19) $H_{T2}/2$ bins in the restricted range of $0.3 < H_{T2}/2 < 1.0$ TeV. For comparison, correlations between the two cross sections are neglected in the simultaneous fit on the left, but fully taken into account in the ratio fit on the right.

PDF set	2- & 3-jets			R_{32}		
	$\alpha_s(M_Z)$	$\pm\Delta\alpha_s(M_Z)$	χ^2/n_{dof}	$\alpha_s(M_Z)$	$\pm\Delta\alpha_s(M_Z)$	χ^2/n_{dof}
CT10	0.1170	0.0026	8.2/37	0.1141	0.0028	19./18
CT14	0.1161	0.0029	9.1/37	0.1139	0.0032	15./18
MSTW2008	0.1161	0.0021	11./37	0.1150	0.0023	21./18
MMHT2014	0.1168	0.0025	11./37	0.1142	0.0022	19./18
NNPDF2.3	0.1188	0.0019	15./37	0.1184	0.0021	12./18

To investigate how the EWK corrections affect the fit results for $\alpha_s(M_Z)$, the range in $H_{T2}/2$ is extended to $0.3 < H_{T2}/2 < 1.68$ TeV. Table 5 reports the values obtained for $\alpha_s(M_Z)$ from fits to the 2-jet event cross section in this range with or without EWK correction factors. The largest impact is a reduction in χ^2/n_{dof}, which indicates a better agreement when EWK effects are included. In addition, a tendency to slightly smaller $\alpha_s(M_Z)$ values is observed without the EWK corrections. For the ratio R_{32} it is expected that these effects are much reduced.

From Fig. 11 follows that only the PDF sets MSTW2008 and MMHT2014 provide a large enough range in $\alpha_s(M_Z)$ values to ensure fits without extrapolation. The other three PDF sets are at the limit such that reliable fits cannot be performed for all scale settings and/or bins in scale

Table 5: Determination of $\alpha_s(M_Z)$ from the inclusive 2-jet event cross section using five PDF sets at NLO with (right) and without (left) EWK corrections. Only total uncertainties without scale variations are quoted. The results are obtained from a simultaneous fit to all 29 $H_{T2}/2$ bins in the range of $0.3 < H_{T2}/2 < 1.68$ TeV.

PDF set	2-jets, without EWK			2-jets, with EWK		
	$\alpha_s(M_Z)$	$\pm\Delta\alpha_s(M_Z)$	χ^2/n_{dof}	$\alpha_s(M_Z)$	$\pm\Delta\alpha_s(M_Z)$	χ^2/n_{dof}
CT10	0.1163	0.0034	15./28	0.1165	0.0032	14./28
CT14	0.1137	0.0033	24./28	0.1144	0.0033	17./28
MSTW2008	0.1093	0.0028	27./28	0.1133	0.0023	19./28
MMHT2014	0.1127	0.0032	32./28	0.1141	0.0032	21./28
NNPDF2.3	0.1162	0.0024	31./28	0.1168	0.0024	23./28

$Q = H_{T2}/2$. Tables 6–8 give the complete results for MSTW2008 and MMHT2014 for the full range in $H_{T2}/2$ of 300 GeV up to 1.68 TeV, for scale variations in this range, and for subranges in $H_{T2}/2$.

Using the MSTW2008 PDF set, which dates from before the LHC start, the strong coupling constant finally is determined to

$$\alpha_s(M_Z) = 0.1150 \pm 0.0010\,(\mathrm{exp}) \pm 0.0013\,(\mathrm{PDF}) \pm 0.0015\,(\mathrm{NP}) {}^{+0.0050}_{-0.0000}\,(\mathrm{scale})$$
$$= 0.1150 \pm 0.0023\,(\text{all except scale}) {}^{+0.0050}_{-0.0000}\,(\mathrm{scale}).$$

The MMHT2014 PDF set, although using LHC jet data to determine the PDF parameters, leads to a very similar result of

$$\alpha_s(M_Z) = 0.1142 \pm 0.0010\,(\mathrm{exp}) \pm 0.0013\,(\mathrm{PDF}) \pm 0.0014\,(\mathrm{NP}) {}^{+0.0049}_{-0.0006}\,(\mathrm{scale})$$
$$= 0.1142 \pm 0.0022\,(\text{all except scale}) {}^{+0.0049}_{-0.0006}\,(\mathrm{scale}).$$

In contrast to fits at NLO using cross sections, where the scale uncertainty recipe usually leads to a very asymmetric behaviour with the larger uncertainty towards smaller values of $\alpha_s(M_Z)$, this is inverted for the fits to the cross section ratio.

Table 9 provides in addition to the extracted $\alpha_s(M_Z)$ value for each range in $H_{T2}/2$ the $\alpha_S(Q)$ values with total uncertainty as evolved to the respective cross-section averaged scale $\langle Q \rangle$ in that range. The evolution is performed for five flavours at 2-loop order with the RUNDEC program [50, 51]. The obtained $\alpha_S(Q)$ points are illustrated in Fig. 12 together with the world average [52] and results from other measurements of the CMS [11, 12, 26, 48, 53], ATLAS [54], D0 [55,56], H1 [57, 58], and ZEUS [59] experiments.

7 Summary

A measurement of the inclusive 2-jet (3-jet) event cross sections has been presented in a range of $0.3 < H_{T2}/2 < 2.0$ TeV ($0.3 < H_{T2}/2 < 1.68$ TeV) for the average p_T of the two leading jets at central rapidity of $|y| < 2.5$. The data sample has been collected from proton-proton collisions at 8 TeV centre-of-mass energy and corresponds to an integrated luminosity of 19.7 fb^{-1}. The data are found to be well described by calculations at NLO in pQCD complemented with NP corrections that are important at low $H_{T2}/2$. The upwards trend seen in the 2- and 3-jet data at high $H_{T2}/2$ in comparison to the prediction at NLO QCD, is explained by the onset of EWK

Table 9: Evolution of the strong coupling constant between the scale of the Z boson mass and the cross-section averaged $H_{T2}/2$ scale $\langle Q \rangle$ for the separate determinations in each respective $H_{T2}/2$ bins in the full fit range. The evolution is performed for five flavours at 2-loop order with the RUNDEC program [50, 51].

$H_{T2}/2$ (GeV)	$\langle Q \rangle$ (GeV)	$\alpha_s(M_Z)$	$\alpha_S(Q)$	No. of data points	χ^2/n_{dof}
300–420	340	$0.1157^{+0.0060}_{-0.0030}$	$0.0969^{+0.0041}_{-0.0030}$	4	2.8/3
420–600	476	$0.1153^{+0.0062}_{-0.0025}$	$0.0928^{+0.0039}_{-0.0016}$	6	6.1/5
600–1000	685	$0.1134^{+0.0059}_{-0.0028}$	$0.0879^{+0.0035}_{-0.0017}$	9	7.1/8
1000–1680	1114	$0.1147^{+0.0074}_{-0.0040}$	$0.0841^{+0.0039}_{-0.0021}$	10	5.4/9

CMS *Preliminary*

- CMS R_{32} preliminary, $\sqrt{s}=8$ TeV, $\alpha_s(M_Z)=0.1150^{+0.0055}_{-0.0023}$
- CMS R_{32} preliminary, $\sqrt{s}=8$ TeV
- CMS Incl.Jet., $\sqrt{s}=8$ TeV
- CMS R_{32}, $\sqrt{s}=7$ TeV
- CMS Incl.Jet., $\sqrt{s}=7$ TeV
- CMS $t\bar{t}$, $\sqrt{s}=7$ TeV
- CMS 3-Jet Mass, $\sqrt{s}=7$ TeV
- ATLAS TEEC, $\sqrt{s}=7$ TeV
- D0 Incl.Jet
- D0 Angular Correlation
- H1
- ZEUS
- World Avg $\alpha_s(M_Z)=0.1181\pm0.0011$

$\alpha_S(Q)$ — Q (GeV)

Figure 12: The running $\alpha_s(Q)$ as a function of the scale Q is shown as obtained by using the MSTW2008 NLO PDF set. The solid line and the uncertainty band are drawn by evolving the extracted $\alpha_s(M_Z)$ values using the 2-loop 5-flavour renormalization group equations as implemented in RUNDEC [50, 51]. The dashed line represents the evolution of the world average [52] and the black circles correspond to the $\alpha_s(Q)$ determinations presented in Table 9. Results from other measurements of CMS [11, 12, 26, 48, 53], ATLAS [54], D0 [55, 56], H1 [57, 58], and ZEUS [59] are superimposed.

Table 6: Determination of $\alpha_s(M_Z)$ from the ratio R_{32} using the two most compatible PDF sets MSTW2008 and MMHT2014 at NLO. The results are obtained from a simultaneous fit to all 29 $H_{T2}/2$ bins in the full range of $0.3 < H_{T2}/2 < 1.68$ TeV.

PDF set	$\alpha_s(M_Z)$	exp	PDF	NP	all exc. scale	scale	χ^2/n_{dof}
			$R_{32}: \Delta\alpha_s(M_Z) \times 1000$				
MSTW2008	0.1150	±10	±13	±15	±23	$^{+50}_{-0}$	26./28
MMHT2014	0.1142	±10	±13	±14	±22	$^{+49}_{-6}$	24./28

Table 7: Fitted values of $\alpha_s(M_Z)$ using R_{32} in the $H_{T2}/2$ range from 0.3 up to 1.68 TeV at the central scale and for the six scale factor combinations for the two PDF sets MSTW2008 and MMHT2014.

$\mu_r/H_{T2}/2$	$\mu_f/H_{T2}/2$	MSTW2008 $\alpha_s(M_Z)$	χ^2/n_{dof}	MMHT2014 $\alpha_s(M_Z)$	χ^2/n_{dof}
1	1	0.1150	26./28	0.1142	24./28
1/2	1/2	0.1165	77./28	0.1160	73./28
2	2	0.1200	18./28	0.1191	18./28
1/2	1	0.1150	53./28	0.1136	48./28
1	1/2	0.1150	30./28	0.1142	28./28
1	2	0.1155	23./28	0.1147	22./28
2	1	0.1180	19./28	0.1175	19./28

Table 8: Uncertainty composition for $\alpha_s(M_Z)$ from the determination of α_s from the jet event rate R_{32} in bins of $H_{T2}/2$. The statistical uncertainty of the NLO computation is negligible in comparison to any of the other sources of uncertainty. Electroweak corrections, significant only at high $H_{T2}/2$, are assumed to cancel between the numerator and denominator.

$H_{T2}/2$ (GeV)	MSTW2008: $\Delta\alpha_s(M_Z) \times 1000$					MMHT2014: $\Delta\alpha_s(M_Z) \times 1000$				
	$\alpha_s(M_Z)$	exp	PDF	NP	scale	$\alpha_s(M_Z)$	exp	PDF	NP	scale
300–420	0.1157	±15	±14	±19	$^{+53}_{-0}$	0.1158	±14	±10	±19	$^{+52}_{-0}$
420–600	0.1153	±11	±14	±18	$^{+57}_{-0}$	0.1154	±11	±12	±17	$^{+56}_{-0}$
600–1000	0.1134	±13	±16	±19	$^{+52}_{-0}$	0.1140	±12	±12	±18	$^{+45}_{-0}$
1000–1680	0.1147	±29	±17	±18	$^{+63}_{-11}$	0.1154	±25	±14	±15	$^{+56}_{-11}$
300–1680	0.1150	±10	±13	±15	$^{+50}_{-0}$	0.1142	±10	±13	±14	$^{+49}_{-6}$

corrections in the 2-jet case. For the 3-jet event cross section these correction have not yet been computed.

In the 3-jet to 2-jet cross section ratio the EWK corrections are assumed to cancel. In fact, NLO QCD provides an adequate description of R_{32} in the accessible range of $H_{T2}/2$. In contrast, LO tree-level MC predictions exhibit significant deviations.

Based on the observed agreement, the strong coupling constant is determined in a fit to the R_{32} measurement to

$$\alpha_s(M_Z) = 0.1150 \pm 0.0010(\text{exp}) \pm 0.0013(\text{PDF}) \pm 0.0015(\text{NP})\,{}^{+0.0050}_{-0.0000}(\text{scale})$$
$$= 0.1150 \pm 0.0023(\text{all except scale})\,{}^{+0.0050}_{-0.0000}(\text{scale})$$

using the MSTW2008 PDF set. Employing the MMHT2014 PDF set instead leads to very similar results. Equally compatible determinations of $\alpha_s(M_Z)$ are achieved with separate fits to the inclusive 2-jet and 3-jet event cross sections employing various PDF sets provided the range in $H_{T2}/2$ is restricted to $0.3 < H_{T2}/2 < 1.0$ TeV. The result for $\alpha_s(M_Z)$ is in agreement with previous determinations obtained by the ATLAS and CMS collaborations [11, 12, 26, 48, 53, 54] and with the world average value of $\alpha_s(M_Z) = 0.1181 \pm 0.0011$ derived in Ref. [52].

References

[1] ALICE Collaboration, "Measurement of the inclusive differential jet cross section in pp collisions at $\sqrt{s} = 2.76$ TeV", *Phys. Lett. B* **722** (2013) 262, doi:10.1016/j.physletb.2013.04.026, arXiv:1301.3475.

[2] ATLAS Collaboration, "Measurement of inclusive jet and dijet cross sections in proton-proton collisions at 7 TeV centre-of-mass energy with the ATLAS detector", *Eur. Phys. J. C* **71** (2011) 1512, doi:10.1140/epjc/s10052-010-1512-2, arXiv:1009.5908.

[3] ATLAS Collaboration, "Measurement of inclusive jet and dijet production in pp collisions at $\sqrt{s} = 7$ TeV using the ATLAS detector", *Phys. Rev. D* **86** (2012) 014022, doi:10.1103/PhysRevD.86.014022, arXiv:1112.6297.

[4] ATLAS Collaboration, "Measurement of the inclusive jet cross section in pp collisions at $\sqrt{s} = 2.76$ TeV and comparison to the inclusive jet cross section at $\sqrt{s} = 7$ TeV using the ATLAS detector", *Eur. Phys. J. C* **73** (2013) 2509, doi:10.1140/epjc/s10052-013-2509-4, arXiv:1304.4739.

[5] ATLAS Collaboration, "Measurement of the inclusive jet cross-section in proton-proton collisions at $\sqrt{s} = 7$ TeV using 4.5 fb^{-1} of data with the ATLAS detector", *JHEP* **02** (2015) 153, doi:10.1007/JHEP02(2015)153, arXiv:1410.8857.

[6] CMS Collaboration, "Measurement of the Inclusive Jet Cross Section in pp Collisions at $\sqrt{s} = 7$ TeV", *Phys. Rev. Lett.* **107** (2011) 132001, doi:10.1103/PhysRevLett.107.132001, arXiv:1106.0208.

[7] CMS Collaboration, "Measurement of the inclusive production cross sections for forward jets and for dijet events with one forward and one central jet in pp collisions at $\sqrt{s} = 7$ TeV", *JHEP* **06** (2012) 036, doi:10.1007/JHEP06(2012)036, arXiv:1202.0704.

[8] CMS Collaboration, "Measurements of differential jet cross sections in proton-proton collisions at $\sqrt{s} = 7$ TeV with the CMS detector", *Phys. Rev. D* **87** (2013) 112002, doi:10.1103/PhysRevD.87.112002, arXiv:1212.6660.

[9] CMS Collaboration, "Measurement of the ratio of inclusive jet cross sections using the anti-k_T algorithm with radius parameters $R = 0.5$ and 0.7 in pp collisions at $\sqrt{s} = 7$ TeV", *Phys. Rev. D* **90** (2014) 072006, doi:10.1103/PhysRevD.90.072006, arXiv:1406.0324.

[10] CMS Collaboration, "Measurement of the double-differential inclusive jet cross section in proton-proton collisions at $\sqrt{s} = 13$ TeV", *Eur. Phys. J. C* **76** (2016), no. 8, 451, doi:10.1140/epjc/s10052-016-4286-3, arXiv:1605.04436.

[11] CMS Collaboration, "Measurement and QCD analysis of double-differential inclusive jet cross-sections in pp collisions at $\sqrt{s} = 8$ TeV and ratios to 2.76 and 7 TeV", (2016). arXiv:1609.05331. Submitted to *JHEP*.

[12] CMS Collaboration, "Measurement of the ratio of the inclusive 3-jet cross section to the inclusive 2-jet cross section in pp collisions at $\sqrt{s} = 7$ TeV and first determination of the strong coupling constant in the TeV range", *Eur. Phys. J. C* **73** (2013) 2604, doi:10.1140/epjc/s10052-013-2604-6, arXiv:1304.7498.

[13] M. Cacciari, G. P. Salam, and G. Soyez, "The anti-k_t jet clustering algorithm", *JHEP* **04** (2008) 063, doi:10.1088/1126-6708/2008/04/063, arXiv:0802.1189.

[14] CMS Trigger and Data Acquisition Group Collaboration, "The CMS high level trigger", *Eur. Phys. J. C* **46** (2006) 605, doi:10.1140/epjc/s2006-02495-8, arXiv:hep-ex/0512077.

[15] CMS Collaboration, "Particle-Flow Event Reconstruction in CMS and Performance for Jets, Taus, and MET", technical report, CERN, 2009.

[16] CMS Collaboration, "Particle-flow commissioning with muons and electrons from J/Psi and W events at 7 TeV", technical report, CERN, 2010.

[17] M. Cacciari, G. P. Salam, and G. Soyez, "FastJet User Manual", *Eur. Phys. J. C* **72** (2012) 1896, doi:10.1140/epjc/s10052-012-1896-2, arXiv:1111.6097.

[18] CMS Collaboration, "Jet energy scale and resolution in the CMS experiment in pp collisions at 8 TeV", (2016). arXiv:1607.03663. Submitted to *JINST*.

[19] T. Sjöstrand, S. Mrenna, and P. Z. Skands, "PYTHIA 6.4 Physics and Manual", *JHEP* **05** (2006) 026, doi:10.1088/1126-6708/2006/05/026, arXiv:hep-ph/0603175.

[20] CMS Collaboration, "Charged particle multiplicities in pp interactions at $\sqrt{s}$ = 0.9, 2.36, and 7 TeV", *JHEP* **01** (2011) 079, doi:10.1007/JHEP01(2011)079, arXiv:1011.5531.

[21] S. Agostinelli et al., "GEANT4: A Simulation toolkit", *Nuclear Instruments & Methods in Physics Research A* **506** (2003) 250, doi:10.1016/S0168-9002(03)01368-8.

[22] CMS Collaboration, "Description and performance of track and primary-vertex reconstruction with the CMS tracker", *JINST* **9** (2014), no. 10, P10009, doi:10.1088/1748-0221/9/10/P10009, arXiv:1405.6569.

[23] CMS Collaboration, "Jet Performance in pp Collisions at $\sqrt{s}$ = 7TeV", technical report, CERN, 2010.

[24] G. D'Agostini, "A Multidimensional unfolding method based on Bayes' theorem", *Nucl. Instrum. Meth. A* **362** (1995) 487, doi:10.1016/0168-9002(95)00274-X.

[25] T. Adye, "Unfolding algorithms and tests using RooUnfold", in *Proceedings, PHYSTAT 2011 Workshop on Statistical Issues Related to Discovery Claims in Search Experiments and Unfolding*, p. 313. Geneva, Switzerland, January 17-20, 2011. arXiv:1105.1160. doi:10.5170/CERN-2011-006.

[26] CMS Collaboration, "Measurement of the inclusive 3-jet production differential cross section in proton-proton collisions at 7 TeV and determination of the strong coupling constant in the TeV range", *Eur. Phys. J. C* **75** (2015) 186, doi:10.1140/epjc/s10052-015-3376-y, arXiv:1412.1633.

[27] CMS Collaboration, "CMS Luminosity Based on Pixel Cluster Counting - Summer 2013 Update", technical report, CERN, 2013.

[28] Z. Nagy, "Three jet cross-sections in hadron hadron collisions at next-to-leading order", *Phys. Rev. Lett.* **88** (2002) 122003, doi:10.1103/PhysRevLett.88.122003, arXiv:hep-ph/0110315.

[29] Z. Nagy, "Next-to-leading order calculation of three-jet observables in hadron hadron collisions", *Phys. Rev. D* **68** (2003) 094002, doi:10.1103/PhysRevD.68.094002, arXiv:hep-ph/0307268.

[30] D. Britzger, K. Rabbertz, F. Stober, and M. Wobisch, "New features in version 2 of the fastNLO project", in *Proceedings, XX. International Workshop on Deep-Inelastic Scattering and Related Subjects (DIS 2012)*, p. 217. Bonn, Germany, March 26-30, 2012. arXiv:1208.3641. doi:10.3204/DESY-PROC-2012-02/165.

[31] A. Buckley et al., "LHAPDF6: parton density access in the LHC precision era", *Eur. Phys. J. C* **75** (2015) 132, doi:10.1140/epjc/s10052-015-3318-8, arXiv:1412.7420.

[32] CMS Collaboration, "Measurement of the inclusive jet cross section in pp collisions at $\sqrt{s}$ = 2.76 TeV", *Eur. Phys. J. C* **76** (2016) 265, doi:10.1140/epjc/s10052-016-4083-z, arXiv:1512.06212.

[33] S. Alekhin, J. Blümlein, and S. Moch, "Parton Distribution Functions and Benchmark Cross Sections at NNLO", *Phys. Rev. D* **86** (2012) 054009, doi:10.1103/PhysRevD.86.054009, arXiv:1202.2281.

[34] H.-L. Lai et al., "New parton distributions for collider physics", *Phys. Rev. D* **82** (2010) 074024, doi:10.1103/PhysRevD.82.074024, arXiv:1007.2241.

[35] A. D. Martin, W. J. Stirling, R. S. Thorne, and G. Watt, "Parton distributions for the LHC", *Eur. Phys. J. C* **63** (2009) 189, doi:10.1140/epjc/s10052-009-1072-5, arXiv:0901.0002.

[36] A. D. Martin, W. J. Stirling, R. S. Thorne, and G. Watt, "Uncertainties on α_S in global PDF analyses and implications for predicted hadronic cross sections", *Eur. Phys. J. C* **64** (2009) 653, doi:10.1140/epjc/s10052-009-1164-2, arXiv:0905.3531.

[37] R. D. Ball et al., "Parton distributions with LHC data", *Nucl. Phys. B* **867** (2013) 244, doi:10.1016/j.nuclphysb.2012.10.003, arXiv:1207.1303.

[38] S. Dulat et al., "New parton distribution functions from a global analysis of quantum chromodynamics", *Phys. Rev. D* **93** (2016) 033006, doi:10.1103/PhysRevD.93.033006, arXiv:1506.07443.

[39] H1, ZEUS Collaboration, "Combination of measurements of inclusive deep inelastic $e^{\pm}p$ scattering cross sections and QCD analysis of HERA data", *Eur. Phys. J. C* **75** (2015) 580, doi:10.1140/epjc/s10052-015-3710-4, arXiv:1506.06042.

[40] L. Harland-Lang, A. Martin, P. Motylinski, and R. Thorne, "Parton distributions in the LHC era: MMHT 2014 PDFs", *Eur. Phys. J. C* **75** (2015), no. 5, 204, doi:10.1140/epjc/s10052-015-3397-6, arXiv:1412.3989.

[41] NNPDF Collaboration, "Parton distributions for the LHC Run II", *JHEP* **04** (2015) 040, doi:10.1007/JHEP04(2015)040, arXiv:1410.8849.

[42] S. Dittmaier, A. Huss, and C. Speckner, "Weak radiative corrections to dijet production at hadron colliders", *JHEP* **11** (2012) 095, doi:10.1007/JHEP11(2012)095, arXiv:1210.0438.

[43] M. Bähr et al., "Herwig++ Physics and Manual", *Eur. Phys. J. C* **58** (2008) 639, doi:10.1140/epjc/s10052-008-0798-9, arXiv:0803.0883.

[44] P. Nason, "A New method for combining NLO QCD with shower Monte Carlo algorithms", *JHEP* **11** (2004) 040, doi:10.1088/1126-6708/2004/11/040, arXiv:hep-ph/0409146.

[45] S. Frixione, P. Nason, and C. Oleari, "Matching NLO QCD computations with Parton Shower simulations: the POWHEG method", *JHEP* **11** (2007) 070, doi:10.1088/1126-6708/2007/11/070, arXiv:0709.2092.

[46] S. Alioli et al., "Jet pair production in POWHEG", *JHEP* **04** (2011) 081, doi:10.1007/JHEP04(2011)081, arXiv:1012.3380.

[47] CMS Collaboration, "Event generator tunes obtained from underlying event and multiparton scattering measurements", *Eur. Phys. J. C* **76** (2015) 155, doi:10.1140/epjc/s10052-016-3988-x, arXiv:1512.00815.

[48] CMS Collaboration, "Constraints on parton distribution functions and extraction of the strong coupling constant from the inclusive jet cross section in pp collisions at $\sqrt{s} = 7$ TeV", *Eur. Phys. J. C* **75** (2015) 288, doi:10.1140/epjc/s10052-015-3499-1, arXiv:1410.6765.

[49] J. Pumplin et al., "New generation of parton distributions with uncertainties from global QCD analysis", *JHEP* **07** (2002) 012, doi:10.1088/1126-6708/2002/07/012, arXiv:hep-ph/0201195.

[50] K. G. Chetyrkin, J. H. Kuhn, and M. Steinhauser, "RunDec: A Mathematica package for running and decoupling of the strong coupling and quark masses", *Comput. Phys. Commun.* **133** (2000) 43, doi:10.1016/S0010-4655(00)00155-7, arXiv:hep-ph/0004189.

[51] B. Schmidt and M. Steinhauser, "CRunDec: a C++ package for running and decoupling of the strong coupling and quark masses", *Comput. Phys. Commun.* **183** (2012) 1845, doi:10.1016/j.cpc.2012.03.023, arXiv:1201.6149.

[52] C. Patrignani and others (Particle Data Group), "Review of Particle Physics", *Chin. Phys. C* **40** (2016) 100001, doi:10.1088/1674-1137/40/10/100001.

[53] CMS Collaboration, "Determination of the top-quark pole mass and strong coupling constant from the tt̄ production cross section in pp collisions at $\sqrt{s} = 7$ TeV", *Phys. Lett. B* **728** (2014) 496, doi:10.1016/j.physletb.2013.12.009, arXiv:1307.1907.

[54] ATLAS Collaboration, "Measurement of transverse energy-energy correlations in multi-jet events in pp collisions at $\sqrt{s} = 7$ TeV using the ATLAS detector and determination of the strong coupling constant $\alpha_s(m_Z)$", *Phys. Lett. B* **750** (2015) 427, doi:10.1016/j.physletb.2015.09.050, arXiv:1508.01579.

[55] D0 Collaboration, "Determination of the strong coupling constant from the inclusive jet cross section in $p\bar{p}$ collisions at $\sqrt{s} = 1.96$ TeV", *Phys. Rev. D* **80** (2009) 111107, doi:10.1103/PhysRevD.80.111107, arXiv:0911.2710.

[56] D0 Collaboration, "Measurement of angular correlations of jets at $\sqrt{s} = 1.96$ TeV and determination of the strong coupling at high momentum transfers", *Phys. Lett. B* **718** (2012) 56, doi:10.1016/j.physletb.2012.10.003, arXiv:1207.4957.

[57] H1 Collaboration, "Measurement of multijet production in ep collisions at high Q^2 and determination of the strong coupling α_s", *Eur. Phys. J. C* **75** (2015) 65, doi:10.1140/epjc/s10052-014-3223-6, arXiv:1406.4709.

[58] H1 Collaboration, "Measurement of Jet Production Cross Sections in Deep-inelastic ep Scattering at HERA", (2016). arXiv:1611.03421. Submitted to *Eur. Phys. J. C*.

[59] ZEUS Collaboration, "Inclusive-jet photoproduction at HERA and determination of α_s", *Nucl. Phys. B* **864** (2012) 1, doi:10.1016/j.nuclphysb.2012.06.006, arXiv:1205.6153.